Modelling Simul. Mater. Sci. Eng. **17** (2009) 045006 (16pp) doi:10.1088/0965-393/17/4/045006

Evaluation of thermomechanical properties of non-stoichiometric gadolinium doped ceria using atomistic simulations

N Swaminathan and J Qu

G.W. Woodruff School of Mechanical Engineering, Georgia Institute of Technology, Atlanta, GA 30332-0405, USA

Received 29 October 2008, in final form 24 February 2009
Published 24 April 2009
Online at stacks.iop.org/MSMSE/17/045006

Abstract

It is well known that gadolinium doped ceria (GDC), when subjected to reducing conditions, undergoes significant volumetric expansion and changes its elastic stiffness. In this paper, a methodology based on a semi-analytical formulation in conjunction with molecular dynamic (MD) simulation is presented to determine the coefficient of compositional expansion (CCE) and the complete elastic stiffness tensor of two common forms of GDC at various levels of non-stoichiometry and temperatures. The CCE is determined by comparing the volumes of the MD simulation cell before and after the reduction at a given temperature. To compute the elastic constants, MD simulations are first conducted to determine the equilibrium (relaxed) positions of each atom. Then, the constants are obtained through an analytical method that uses the relaxed positions of the atoms in the simulation cell. It is found that the elastic stiffness tensor of the non-stoichiometric structures remain cubic. The elastic constant C_{11} decreases with increasing vacancy concentration, while the changes in C_{12} and C_{66} were found to be negligible. In addition, both the elastic constants and the CCE are found to be insensitive to temperature.

1. Introduction

Gadolinium doped ceria (GDC) undergoes a significant chemical expansion [1, 2] and also shows a decrease in its elastic stiffness [3] due to the increase in oxygen vacancies in a reducing environment. The effect of this chemical change on the mechanical response can be quantified by a set of material properties known as coefficient of compositional expansion (CCE) and open system elastic constants (OSECs), if the deviation from stoichiometry is not too large. In this case, the CCE, denoted by η, is defined as the linear strain per deviation from stoichiometry [4], i.e.

$$\eta = \left.\frac{\partial \varepsilon_{\mathrm{L}}}{\partial \rho}\right|_{\rho=\rho_0}, \tag{1}$$

0965-0393/09/045006+16$30.00

where ε_L is the linear strain, ρ is the vacancy concentration, ρ_0 is the stoichiometric concentration of vacancies so that $\delta = \rho - \rho_0$ is the deviation from stoichiometry.

Similarly the OSEC, $C_{ijkl}(\rho)$ describes the dependence of elastic constants on the local composition of the material. The term was first introduced by Larche and Cahn [5] to describe the composition-dependent elastic constants in metallic materials.

The importance of the CCE lies in the fact that non-uniform distributions of point defects, like vacancies [6, 7], are always present in solid electrolytes used in fuel cell applications. The presence of such point defects causes local volumetric strains. When these inhomogeneous strains are not accommodated through an appropriate deformation, mechanical stresses result causing failure of the electrolyte [8]. Such effects have been modeled and studied for alloy systems by Larche and Cahn [5, 9–14]. The work of Larche and Cahn was extended to ionic crystals by Johnson in [15, 16]. In a recent paper the present authors have developed a theory for coupling electrochemistry and mechanics in ionic solids [4]. In this coupled theory, the CCE and OSEC are key material parameters that provide the coupling between electrochemistry and mechanical stresses. Therefore, in order to utilize the coupled theory, the CCE and OSEC need to be determined.

Determination of the CCE in ceria or doped ceria and other lanthanum-based compounds has been studied by a number of researchers [17–21]. Most of these works involved physical experiments to measure the stoichiometry and the volumetric expansion. On the other hand, determining OSEC is not as straightforward. Only a few results are available [3, 22, 23]. In these works, a simple analytical expression of the Young's modulus was derived as a function of the vacancy concentration. This was obtained based on a Lennard-Jones type of pair potential. Although the analytical expressions derived in these works provide a trend in the variation of modulus with non-stoichiometry, parameters in the formula must be determined empirically by fitting to the experimental data.

In this paper, molecular dynamics (MD) is used directly to compute CCE. MD is also used to determine the equilibrium positions of all the atoms in a MD simulation cell at various temperatures. This information is then used in an analytical formulation to compute OSEC. Although results are presented here only for two common forms of GDC under various states of non-stoichiometry and temperatures, the methodology itself can be easily applied to other ionic solids of interest. In addition to reporting the data on CCE and the full set of OSEC, we will also examine how the long (coulombic) and short-range parts of the interatomic potential contribute to the OSEC as the vacancy concentration increases.

As a numerical simulation tool, MD has been used to study ceria and doped ceria for several purposes including determining the coefficient of thermal expansion (CTE) [24] and studying the effect of various dopants on its properties [25]. It has, however, not been used to determine the CCE and OSEC for the ionic compound. In the next section we first briefly describe the interatomic potential used, analyze non-stoichiometry in GDC and specify the MD simulation parameters. In the subsequent section detailed results are presented for the CCE. Then, explicit expressions are shown and used to calculate the OSEC contributions. Finally, the paper is concluded with a summary.

2. Molecular dynamic simulations

2.1. Interatomic potentials and simulation conditions

In this work, we use DL-POLY to perform the MD simulations [26]. Buckingham potential is used where the energy due to short-range interaction is given by

$$U^{(n)} = A \exp\left(-\frac{r^{mn}}{\rho}\right) - \frac{C}{(r^{mn})^6}, \tag{2}$$

Table 1. Interatomic potential parameters for the Buckingham potential.

Ionic pairs	A (eV)		ρ (Å)		C (eV Å^6)	
O^{2-}–O^{2-}	9547.96[a]	9533.421[b]	0.2192[a]	0.234[b]	32.0[a]	224.88[b]
Ce^{4+}–O^{2-}	1809.68[a]	755.1311[b]	0.3547[a]	0.0[b]	20.40[a]	0.0[b]
Ce^{3+}–O^{2-}	2010.18[a]	1140.193[b]	0.3449[a]	0.386[b]	23.11[a]	0.0[b]
Gd^{3+}–O^{2-}	1885.75[c]		0.3399[c]		20.34[c]	

[a] Parameters from [27].
[b] Parameters from [28].
[c] Parameters from [29].

where r^{mn} is the scalar distance between atom m and atom n. The parameters A, ρ and C are listed in table 1, where two sets of potential parameters for the ionic pairs Ce^{4+}–O^2, O^{2-}–O^{2-} and Ce^{3+}–O^{2-} are also listed. The first set of parameters of pure ceria taken from [27] are known to predict the lattice parameters, lattice energies, static relative permittivity and high frequency dielectric constant of pure ceria with good accuracy. Although this set of parameters predicts the CCE accurately, they overestimate the elastic constants by as much as 50% for pure ceria at its stoichiometric state, when compared with existing experimental data in the literature. The second set of potential parameters taken from [28] were obtained by fitting the elastic properties of ceria. Therefore, they tend to predict good results for OSEC, but not for CCE. For the above reasons, results for CCE and OSEC are computed using the first [28] and second [29] set of potential parameters, respectively. The potential parameters for the Gd^{3+}–O^{2-} pair were taken from [29] where they were used to study defect clusters in doped ceria.

The cut off radius for the short-range forces was set to 16.0 Å in all simulations. Further, all the electrostatic interactions were computed using Ewald's sum with complete charges being assigned to the specific ions i.e. +4 or +3 for Ce (depending on whether it is Ce^{4+} or Ce^{3+}), +3 for Gd and −2 for O.

In simulations involving point defects in ionic solids it is important to consider the core–shell interactions to capture the possible polarization of the ions (see e.g. [29]). In the current work the core–shell interaction was not considered on account of the following three observations.

(1) MD calculations of elastic constants of pure ceria, for which experimental data exist, show negligible error when the core–shell potentials were neglected.
(2) CCE and OSEC computed in this work for the two forms of GDC are also shown in later sections to match experimental data with reasonable accuracy even when the core–shell interaction was neglected.
(3) Implementation of the core–shell interactions is computationally intensive for the small improvement in the numerical estimate it is going to contribute in this particular case.

All simulations were performed in an NST (constant stress) ensemble so as to allow for variation in MD cell shape, which may take place due to non-stoichiometry. Further, the total period of equilibration was 3 ps and the production run was carried out for 5 ps with a time step of 0.1 fs. The total simulation time was found to be sufficiently long by checking the thermodynamic parameters of the system for convergence. Further, to ensure that the atoms have reached their equilibrium positions a simple test was performed. Since, it is well known that the oxygen atoms have the highest diffusion coefficient in the defective GDC lattice, their positions were continuously monitored during the simulation. It was found that, at the end of 5 ps the oxygen atoms showed no significant displacement from their lattice sites, indicating that they had reached their equilibrium positions in the lattice.

Finally, it is important to point out that the main purpose of the MD simulation is to compute the cell volume (needed for computing CCE) and the atom position (needed for computing OSEC). These quantities were obtained by averaging the cell volumes and atom positions, respectively, over time during the production run of the MD simulations. In essence the MD simulation is to provide a self-equilibrium state of the cell at a given temperature (this could have been done by a molecular static simulation if the thermal expansion of the cell is known). Such equilibrium state at each given temperature is then used in an analytical formulation to compute the OSEC. This semi-analytical method has proven to be accurate for computing elastic properties of FCC metals [30]. We also found that it predicts the elastic constants of pure ceria accurately.

2.2. Non-stoichiometric GDC MD simulation cell

Oxygen ion conductors like GDC are obtained by doping the parent compound (e.g. Ceria, CeO_2) with aliovalent compounds like gadolinia (Gd_2O_3). Such a doping process is represented using the following reaction:

$$Gd_2O_3 \xrightarrow{CeO_2} 2Gd'_{Ce} + V_O^{\bullet\bullet} + 3O_O^X. \tag{3}$$

The charge compensating vacancy concentration (1 oxygen vacancy for every 2 Ce^{4+} ions replaced by Gd^{3+} ions) created as a process of this doping is referred to as the stoichiometric vacancy concentration in the compound. 10GDC and 20GDC are stoichiometric, where gadolinium atoms replace 10% and 20% of the cerium sites in ceria, respectively. Their chemical formulae are written as $Ce_{0.9}Gd_{0.1}O_{2-0.05}$(10GDC) and $Ce_{0.8}Gd_{0.2}O_{2-0.1}$ (20GDC). Note that the subscripts in the formula are in the units of moles per mole of ceria.

Additional vacancy concentration can be created in stoichiomteric GDC when it is exposed to a low partial pressure of oxygen. Such a reducing environment is often encountered in the anodes of SOFC. This reduction is represented using the defect reaction as

$$O_O^X \leftrightarrow V_O^{\bullet\bullet} + 2e' + \tfrac{1}{2}O_2. \tag{4}$$

The above process creates a non-stoichiometric 10/20GDC vacancies, in excess of the stoichiometric compound, and the charges are compensated by reduction of Ce^{4+} to Ce^{3+}. While constructing the MD simulation cell it is important to consider the vacancy concentration created from both the doping and the reduction. This is briefly described below.

To analyze non-stoichiometry in the GDC MD simulation cell, let us suppose that there are x number of Ce^{4+} sites and $2x$ numbers of O^{2-} sites (this corresponds to pure ceria) in the MD cell. We want to generate a structure corresponding to the formula $Ce_{0.9}Gd_{0.1}O_{2-0.05-y}$. Firstly, we recognize that, this compound is non-stoichiometric 10GDC with y mole fraction of vacancy concentration in excess of the stoichiometric compound ($Ce_{0.9}Gd_{0.1}O_{2-0.05}$). Hence, the total number of oxygen atoms to be removed to create the N_v number of vacancies is

$$N_v = (0.05 + y)\,x. \tag{5}$$

The total number of Ce^{4+} positions to be replaced by Gd^{3+} is given by

$$N_{Gd^{3+}} = 0.1x. \tag{6}$$

Further, owing to the reduction we need to replace $N_{Ce^{3+}}$of the Ce^{4+} atoms with Ce^{3+} atoms such that the system is electrically neutral; in this case it is

$$N_{Ce^{3+}} = 2yx. \tag{7}$$

This exercise of removing and replacing atoms has to be done within the MD simulation cell to computationally simulate the required level of non-stoichiometry and reduced structure.

However, the manner in which it can be done depends on the physical quantity under consideration. The details of this construction procedure are given in sections 3.1 and 4.1 for the determination of CCE and OSEC, respectively.

To this end, for the determination of both CCE and OSEC, the simulations were all carried out for four different temperatures 100, 900, 1173 and 1273 K for both 10 and 20GDC. The levels of non-stoichiometry examined were $\delta = 0$, 0.05, 0.1, 0.15, 0.2 and 0.25 for $Ce_{0.9}Gd_{0.1}O_{1.95-\delta}$(10GDC) and $Ce_{0.8}Gd_{0.2}O_{1.9-\delta}$ (20GDC).

In closing this section we would like to point out that we have used two references to compare our MD simulation results of the CCE [3] and the elastic constants [31]. In both these references the physical quantity is either plotted or tabulated for various oxygen partial pressures rather than the deviation in vacancy concentration δ. Therefore, in comparing our results with the experiments performed in the appropriate references, we have converted the partial pressure to the deviation values using expression 11 in [3].

3. Coefficient of compositional expansion

3.1. Building the non-stoichiometric MD cell

For the determination of CCE, the MD simulation box reflecting the appropriate level of non-stoichiometry and chemical reduction was generated randomly. First a pure ceria system comprising of 12 000 atomic sites ($x = 4000$) was considered. From this structure the required numbers of oxygen atoms were removed and cerium atoms were replaced according to the procedure given in section 2.2 randomly within the entire MD cell. To this defective MD cell, periodic boundary conditions were imposed to simulate the bulk material.

3.2. CCE-MD simulation results

The MD simulation cell was relaxed in a NST (constant stress) ensemble to allow for any variation in cell shape. After relaxation, the MD cell vectors were examined and it was concluded that the strains induced as a result of non-stoichiometry was purely volumetric. This is in accordance with experimental evidence [32]. Since the deformation is purely volumetric, the linear strain

$$\varepsilon_{\mathrm{L}} = \frac{[V(\delta) - V(0)]}{3V(0)} \tag{8}$$

can be obtained by comparing the volumes of the relaxed MD simulation cells between the non-stoichiometric and stoichiometric states at the same temperature. The results are presented in figure 1 for a range of δ and temperature. The linear dependence between the strain and non-stoichiometry is clearly observed. Thus, it follows from equation (1) that the CCE is obtained from the slopes of these lines, i.e. $\eta = \varepsilon_{\mathrm{L}}/\delta$. The results are shown in table 2.

It is seen that the CCEs are slightly higher for lower temperatures suggesting that the effect of temperature on the CCE is to decrease it. Also, the CCE values are higher for 10GDC than for 20GDC concluding that a higher doping concentration reduces the CCE values. Further, it seems that the CCE for GDC may be approximately considered to be in the range of 0.069–0.079 for a wide range of temperatures.

The value of CCE predicted here compare very well with experimentally measured data for these materials [3], particularly at low vacancy concentrations (figure 1(*c*)). For higher concentrations, the maximum difference between our predictions and the experimental data is less than 10% which is possibly due to the differences in the temperatures between the

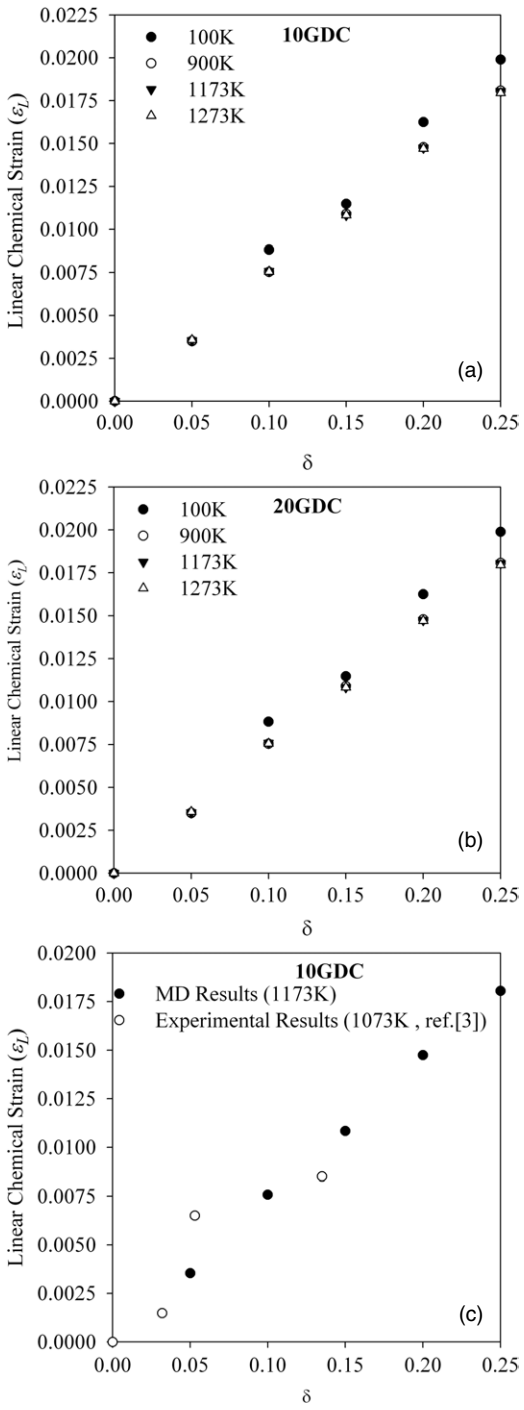

Figure 1. (*a*) Compositional strain versus δ for 10GDC. (*b*) Compositional strain versus δ for 20GDC. (*c*) Comparing MD and experimental results for the variation of linear strain with stoichiometry.

Table 2. Average CCE values for 10 and 20GDC at various temperatures.

	CCE	
Temperature (K)	10GDC	20GDC
100	0.0791	0.0764
900	0.0729	0.0709
1173	0.0729	0.0694
1273	0.0729	0.069

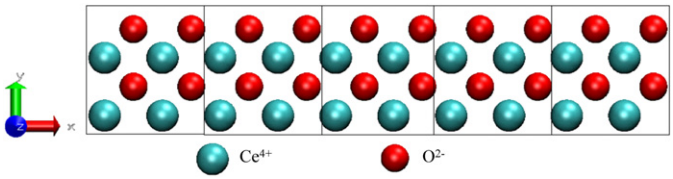

Figure 2. The placement of five unit cells of pure ceria.

MD and the experimental runs. But as pointed out in table 2 the values of the CCEs are not sensitive to temperature and hence the comparison is a good indication of the validity of the results.

4. Open system elastic constants

4.1. Building the non-stoichiometric MD cell

As done for the determination of CCE the removal and replacement of atoms may be done at random within the MD simulation cell. But by doing so, information regarding the kind or the number of sub-lattices present in the system is lost (disorder [33]). Every atom in the system becomes a sub-lattice on its own. As will be explained in the next section, if each atom in the system is considered a sub-lattice, the determination of inner-elastic constants becomes computationally prohibitive.

To address this problem, a hierarchical approach was used in this work. First, a super cell with a given amount of non-stoichiometry was created. To this end, we started with M number of unit cells of pure ceria. Depending on the given level of non-stoichiometry, appropriate number of oxygen atoms are removed, and Ce^{4+} are replaced with Ce^{3+}or Gd^{3+} in this M-cell ceria assembly according to the procedure in section 2.2. The removal and replacement was done randomly within the M-cell ceria assembly. This creates a defective structure with desired level of non-stoichiometry, and will be referred to as the super cell, see figure 2. Clearly, because of the random removal and replacement, there is no periodicity and each atom in the super cell may act as a sub-lattice. In our numerical computations, $M = 5$ was used, which corresponds to 60 atoms or sub-lattices in a super cell. This allows us to create a wide range of non-stoichiometry exactly.

In the second step, super cells are stacked repeatedly in the X, Y and Z directions, respectively, to construct the MD simulation cell. In this work, we used two super cells in the [1 0 0], ten in each of the [0 1 0] and [0 0 1] directions so the MD simulation cell consists of 12 000 atomic spots including vacancies. Periodic boundary conditions are imposed on all three directions of the MD simulation cell to obtain bulk properties.

It should be pointed out that the MD simulation cell constructed above is not unique for several reasons. Firstly, the size of the super cell can vary. We have used $M = 5$. This is large enough for us to study a wide range of non-stoichiometry. Secondly, the structure of the super cell is random. It can be shown that there are literally thousands of ways to create the super cell even for $M = 5$. Further we hasten to add that, if the preferred locations of the vacancies with respect to the dopant atoms are known, the number of possible variants of the super cell can be dramatically reduced. Nevertheless, we assume in this work that any position of vacancy relative to the position of the dopant atom is equally likely. Finally, although some of the atoms in a super cell may not form distinct sub-lattices, they can be treated as if they were, without affecting the results.

4.2. OSEC-simulation results

The determination of OSEC is not as straightforward as the CCE. In this paper, the method of homogenous strains is used to obtain analytical expression for the elastic constants from the interatomic potential [34]. This approach typically neglects the kinetic energy of the atoms, thus gives the elastic constants of the material at 0 K. As discussed below, a modification of this approach is taken in this paper to account for the temperature effect.

The elastic constants of a crystalline solid are given by [35, 36],

$$C_{ijmn} = \hat{C}_{ijmn} + \tilde{C}_{ijmn}, \tag{9}$$

where

$$\hat{C}^{=}_{ijkl} \frac{1}{2\Omega} \sum_{p=1}^{N} \sum_{\substack{q=1 \\ p \neq q}}^{N} \left[\frac{1}{(r^{pq})^2} \left\{ \frac{\partial^2 e\,(r^{pq})}{\partial\,(r^{pq})^2} - \frac{1}{(r^{pq})} \frac{\partial e\,(r^{pq})}{\partial r^{pq}} \right\} \Bigg|_{r=r^0} \right] r_i^{0[pq]} r_j^{0[pq]} r_k^{0[pq]} r_l^{0[pq]} \tag{10}$$

is the average homogeneous part of the elastic constants which describes the elastic response of the crystalline solid when all the atoms are displaced homogeneously upon the application of the strain. In equation (10), $e(r^{pq})$ is the interaction energy between atoms p and q and contains both short-range and the coulombic contributions, N is the total number of atoms in the simulation cell, and Ω is the volume of the MD cell. The jth component of the interatomic distance vector, $r_j^{0[pq]}$, between atoms p and q is measured after the system has fully relaxed at the given temperature of interest. At different temperature, $r_j^{0[pq]}$ is different. Thus, the elastic constants are temperature-dependent.

The second term, $\tilde{C}_{ijkl}$, on the right hand side of equation (9) represents the inhomogeneous part of the elastic constants and relates to the internal relaxation which takes place due to the fact that a minimum energy configuration is attained only when non-equivalent atoms are further displaced relative to each other after the application of the displacement on the boundary of the MD cell corresponding to a uniform strain. This part vanishes for centro-symmetric structures such as monatomic Bravais lattices. For the defective GDC system considered here it is not obvious that this inhomogeneous part is zero and must be considered.

According to [35, 36],

$$\tilde{C}_{ijmn} = -D^k_{ij\alpha} g^{kr}_{\alpha\beta} D^r_{\beta mn}, \tag{11}$$

where the superscripts refer to the sub-lattice and the subscripts refer to tensor components:

$$D^{b}_{uv\alpha} = \frac{1}{2\Omega}\sum_{p=1}^{N}\sum_{\substack{q=1\\ q\neq p}}^{N}\frac{1}{(r^{pq})^2}\left[\frac{\partial^2 e(r^{pq})}{\partial\,(r^{pq})^2} - \frac{1}{(r^{pq})}\frac{\partial e(r^{pq})}{\partial r^{pq}}\right] r_u^{o[pq]} r_v^{o[pq]} r_\alpha^{o[pq]}\left[\delta^{pb} - \delta^{qb}\right], \tag{12}$$

$$B^{bc}_{\alpha\beta} = \frac{1}{2\Omega}\sum_{p=1}^{N}\sum_{\substack{q=1\\ p\neq q}}^{N}\frac{1}{(r^{pq})^2}\left[\frac{\partial^2 e(r^{pq})}{\partial\,(r^{pq})^2} - \frac{1}{(r^{pq})}\frac{\partial e(r^{pq})}{\partial r^{pq}}\right]\left[\delta^{pb} - \delta^{qb}\right]\left[\delta^{pc} - \delta^{qc}\right] r_\alpha^{o[pq]} r_\beta^{o[pq]}$$
$$+\frac{1}{r^{pq}}\frac{\partial e(r^{pq})}{\partial r^{pq}}\delta_{\alpha\beta}\left[\delta^{pb} - \delta^{qb}\right]\left[\delta^{pc} - \delta^{qc}\right] \tag{13}$$

and $g^{th}_{\kappa\lambda}$ is the inverse of $B^{hl}_{\lambda\beta}$, i.e.

$$g^{th}_{\kappa\lambda} B^{hl}_{\lambda\beta} = \delta_{\kappa\beta}\delta^{tl}. \tag{14}$$

In the above, $\delta_{ab} = \delta^{ab}$ is the Kronecker delta.

It can be seen that the matrix $\boldsymbol{B}$ is a 3×3 matrix for every pair of sub-lattices under consideration. In the manner we have constructed, the super cell has at the most 60 sub-lattices and $\boldsymbol{B}$ will be of dimensions 180×180 at the most. In fact for the defective structures it will be even smaller. If all the atoms are considered a sub-lattice, then it is not difficult to imagine the increase in the size of $\boldsymbol{B}$, making the super cell approach computationally more tangible.

4.3. OSEC for single crystal GDC

The single crystal stiffness tensor for the range of non-stoichiometry and temperatures considered are plotted in figure 3. These were calculated based on equation (9). Although the GDC structures were all constructed from ceria which has a cubic symmetry, the GDC crystal no longer has the cubic symmetry structure-wise. Nevertheless, we found that the deviation from cubic response is negligibly small. Therefore, only the three elastic constants C_{11}, C_{12} and C_{66} representing cubic symmetry are reported here, and their variations with non-stoichiometry are plotted in figure 3 for various temperatures.

Figure 3(*a*) shows how C_{11} varies with δ at 100, 900, 1173 and 1273 K for 10GDC. The same is shown in figure 3(*b*) for 20GDC. Similarly, data for C_{66} are shown in figures 3(*c*) and (*d*), and C_{12} in figures 3(*e*) and (*f*) for 10GDC and 20GDC, respectively. The trend obtained in the variation of the elastic constants with non-stoichiometry clearly indicates one important point. The variation is higher for C_{11} than for C_{12} or C_{66}. The C_{11} decreases with an average slope of 400 while the others increase with a slope of 45. The former components fall by about 75–100 GPa over the entire range of non-stoichiometry examined here while the latter ones do not increase more than 10–12 GPa. Possible reasons for this behavior will be analyzed in the section below, where the contributions of the short-range and the long-range terms to the elastic tensor will be examined.

4.4. OSEC for polycrystalline GDC

The elastic constants obtained using the above approach is valid for a single crystal. In general it is well known that the GDC used in electrolytes has a polycrystalline nature. Hence in this section we obtain the polycrystalline properties using a homogenization method. Consider a polycrystalline solid comprising numerous randomly oriented defective single crystal GDC

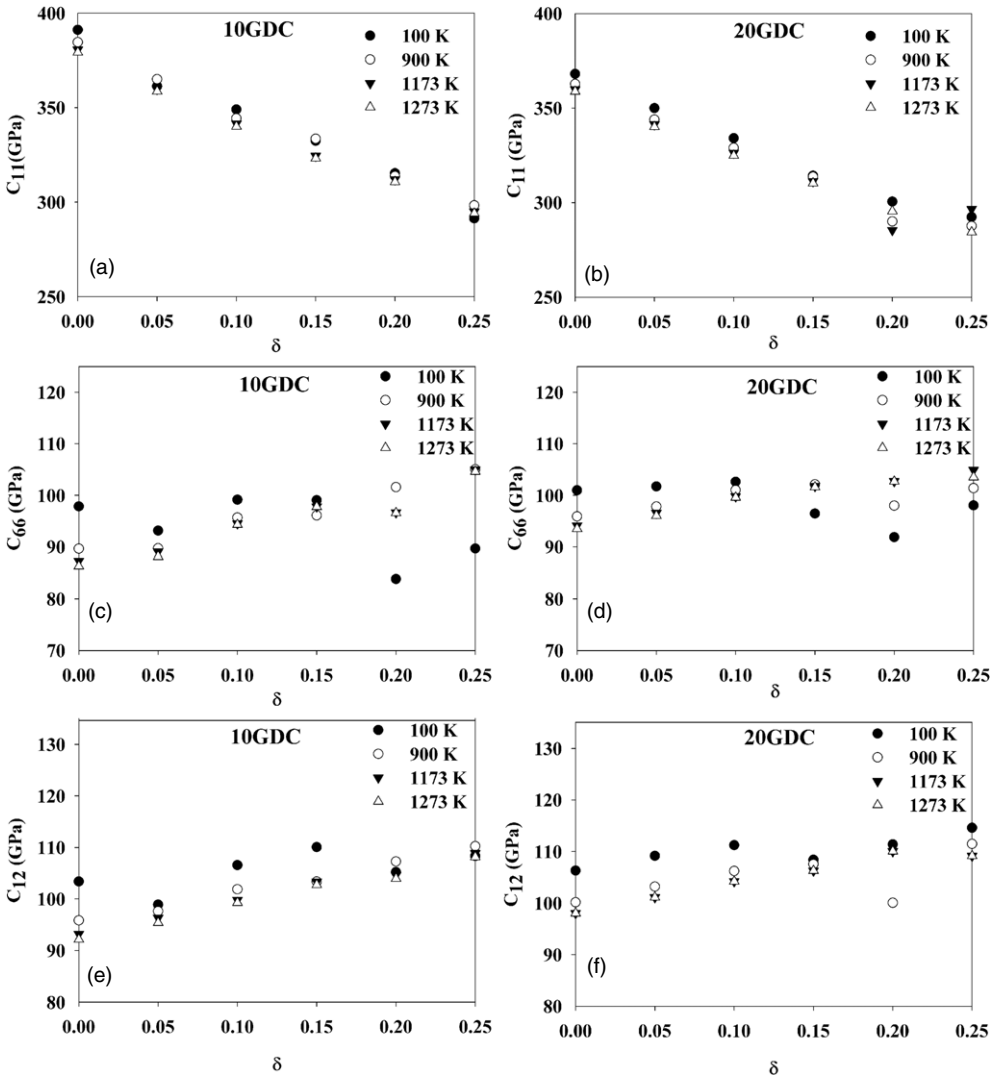

Figure 3. (*a*) and (*b*) Variation of C_{11} with δ for 10GDC and 20GDC, respectively, (*c*) and (*d*) variation of C_{66} with δ for 10 and 20GDC, respectively, (*e*) and (*f*) variation of C_{12} with δ for 10 and 20GDC, respectively.

(grains) as analyzed above. The effective elastic constants for the polycrystalline solid can be obtained by a weighted average of the elastic constants of the individual grains [37]:

$$\bar{C}^{=}_{pqrs} \frac{1}{8\pi^2} \int_0^{2\pi} \mathrm{d}\psi \int_0^{\pi} \sin\theta \mathrm{d}\theta \int_0^{2\pi} f\,(\varphi, \theta, \psi)\alpha_{ip}\alpha_{jq}\alpha_{kr}\alpha_{ls}C_{ijkl}\,\mathrm{d}\varphi, \qquad (15)$$

where θ, φ and ψ are the Euler angles representing the grain orientation and $f(\varphi, \theta, \psi)$ is the probability distribution of the grain orientation. For random orientation, $f(\varphi, \theta, \psi) = 1$.

Due to the random nature of the grain orientation, the effective elastic constants of the polycrystalline solid are isotropic. Therefore, they can be more conveniently represented by the two more familiar engineering elastic constants, Young's modulus and Poisson's ratio [3, 37].

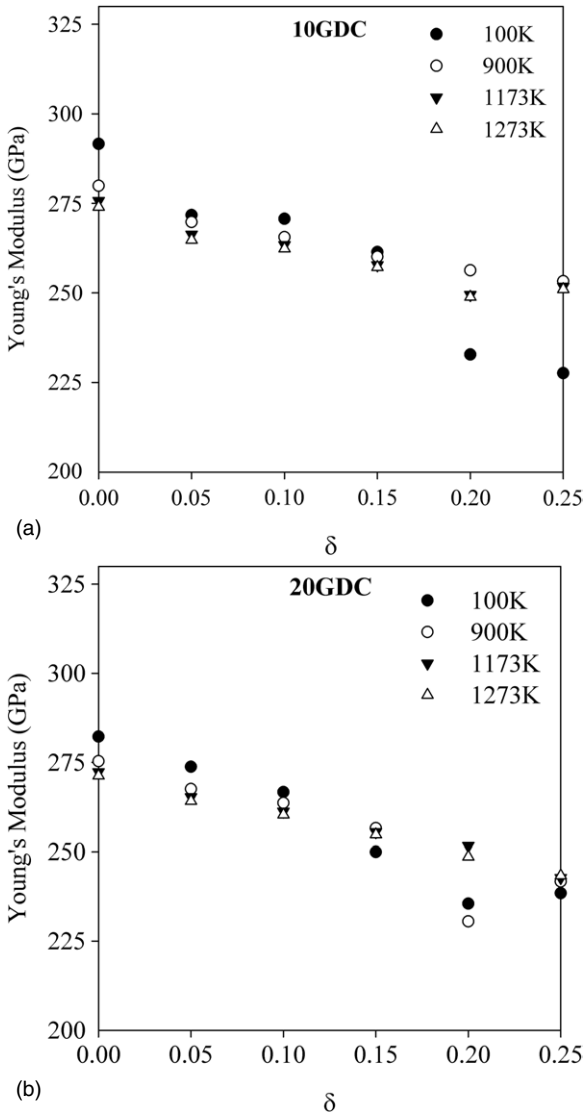

Figure 4. (*a*) Variation of Young's modulus with non-stoichiometry for 10GDC. (*b*) Variation of Young's modulus with non-stoichiometry for 20GDC.

Results for the Young's modulus are plotted in figures 4(*a*) and (*b*), for 10GDC and 20GDC, respectively.

It is again seen that the trend predicted is well approximated by a linear function with a negative slope. Further, it appears from these figures that the Young's modulus by itself and its variation with stoichiometry are not strong functions of temperature.

Although not shown in this paper, it was found that Poisson's ratio is about 0.26 and does not change by more than 4% over the range of temperature and non-stoichiometry considered here.

To verify the accuracy of the numerical estimate, we compare our computed Young's modulus with the experimental data reported in [31] for 10GDC. This is shown in figure 5.

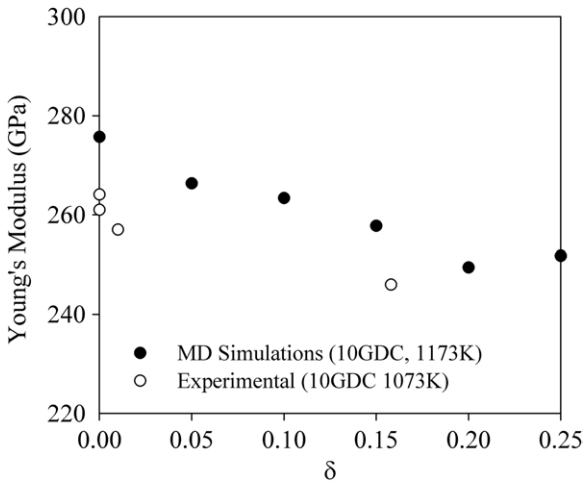

Figure 5. Variation of Young's modulus with non-stoichiometry.

Clearly, both experimental data and our numerical computation indicate the near linear variation of Young's modulus versus non-stoichiometry. Our numerical results tend to slightly over-predict the modulus at higher vacancy concentrations by about 13%. We also speculate that the interatomic potential used here was fit for stoichiometric GDC. It may not predict the elastic properties of non-stoichiometric compound very accurately, especially at higher vacancy concentrations.

4.5. Contribution of inner-elastic constants

Intuitively, one would think that the defective GDC structure far from being centro-symmetric, or monoatomic Bravais lattices would not deform homogeneously even under a homogeneous overall deformation. Thus, the inhomogeneous part of the elastic constants $\tilde{C}_{ijkl}$ would not be negligible. However, our numerical results show that for the ranges of non-stoichiometry and temperature considered here, the contribution from $\tilde{C}_{ijkl}$ is only about 2% for both 10 and 20GDC.

Some authors [38–40] have suggested that defective fluorite structures may be built from fluorite type modules by different arrangements. In particular 22 different basic fluorite type modules were suggested in [38, 39] which could be used to build defective fluorite based oxides that form a homologous series of the form A_nO_{2n-2m} (A—cation, O—Oxygen). These structures built from fluorite type modules are non-primitive and show inner-elastic contribution. The results obtained here seem to indicate that defective ceria structures with several kinds of dopants may not be simply modeled using fluorite type modules. The relaxation of atoms around the vacancies is significant and alters the structure so that the inner-elastic contribution becomes negligibly small.

To test this hypothesis, we also computed the elastic constants of the unrelaxed defective GDC structure. By 'unrelaxed' we mean the structure as built (before the MD run was performed) where all cations are in the Ce^{4+} positions while all the oxygen ions and vacancies are in the O^{2-} position of a perfect fluorite structure. Essentially, the unrelaxed structure comprises of only fluorite modules suggested in [38, 39]. We found that for 20GDC at $\delta = 0.15$ and 1173 K, contributions from $\tilde{C}_{ijkl}$ to the total elastic constants can be as much as over 70%

Table 3. Elastic constant calculations for four trials.

	Elastic constants in 100 GPa					% Variation from the average			
Components	Trial 1	Trial 2	Trial 3	Trial 4	Average	Trial 1	Trial 2	Trial 3	Trial 4
C_{11}	3.02	2.92	3.09	3.10	3.03	0.41	0.11	−0.06	−0.07
C_{22}	3.19	3.24	3.14	3.12	3.17	−0.62	−0.06	0.03	0.05
C_{33}	3.20	3.18	3.28	3.12	3.19	−0.20	0.02	−0.09	0.08
C_{12}	1.07	1.08	1.06	1.08	1.08	0.30	−0.01	0.01	−0.01
C_{13}	1.07	1.07	1.06	1.08	1.07	0.20	0.00	0.01	−0.01
C_{23}	1.08	1.06	1.07	1.09	1.07	−0.26	0.01	0.01	−0.01
C_{44}	1.04	1.01	1.00	1.09	1.03	−0.23	0.03	0.03	−0.05
C_{55}	1.00	1.00	0.96	1.08	1.01	0.98	0.01	0.05	−0.07
C_{66}	1.01	0.98	0.97	1.08	1.01	0.27	0.03	0.04	−0.07

for some of the components. Under the same conditions, $\tilde{C}_{ijkl}$ in the relaxed state contributes only a few percent to the overall elastic constants.

Thus, as a conclusion, we believe that the defective ceria structures may not be properly modeled by using fluorite type modules. The relaxed positions that the atoms take are significantly different from the unrelaxed ones in defective structures and must be accounted for to study the material response. Furthermore, ceria based defective structures (10 and 20GDC) with the vacancy concentrations and dopants examined in the current work behave more like a cubic structure with all the atoms at positions, which are either close to or at inversion centers. Therefore there is very little contribution from inner elasticity.

4.6. Dependence of elastic constants on initial configuration

Another point worth mentioning is whether the initial structure created will lead to the global minimum energy state after relaxation. Because of the complex composition of the material, its energy landscape may have a local minima. An arbitrarily generated initial structure would fall into a local minimum after relaxation, which may then give very different elastic constants each time a new initial structure is used. To verify if this is the case, we generated three different initial structures with $M = 5$ for one specific stoichiometry level and temperature for 10GDC. The OSEC computed from these three initial structures are shown in table 3 in the columns labeled Trial 1–3. It is seen that the results from these three very different initial structures differ by less than 1%. This seems to indicate that the computed OSECs are relatively independent of the initial structure of the simulation cell.

A further verification of the above conclusion is conducted by building an initial MD simulation cell in such a way that all vacancies and the replacement of the ions were carried out completely randomly within the entire MD cell itself (i.e. no super cells were constructed) and no inner elasticity was accounted for. The results are shown in table 3 under the column Trial 4. It is seen that the results differ from those under Trials 1–3 by less than 1%. Recall that the results under the columns Trial 1–3 were obtained using different initial structures within a super cell and accounted for inner elasticity. Data shown in table 3 indicate that the OSEC in the materials considered are independent of both the initial structure and the internal relaxation between different sub-lattices.

4.7. Short-range and coulombic contributions to elastic constants

In this section we investigate the relative contributions of the short-range and the long-range force fields (coulombic interactions) to the total elastic constants of the compound. All the

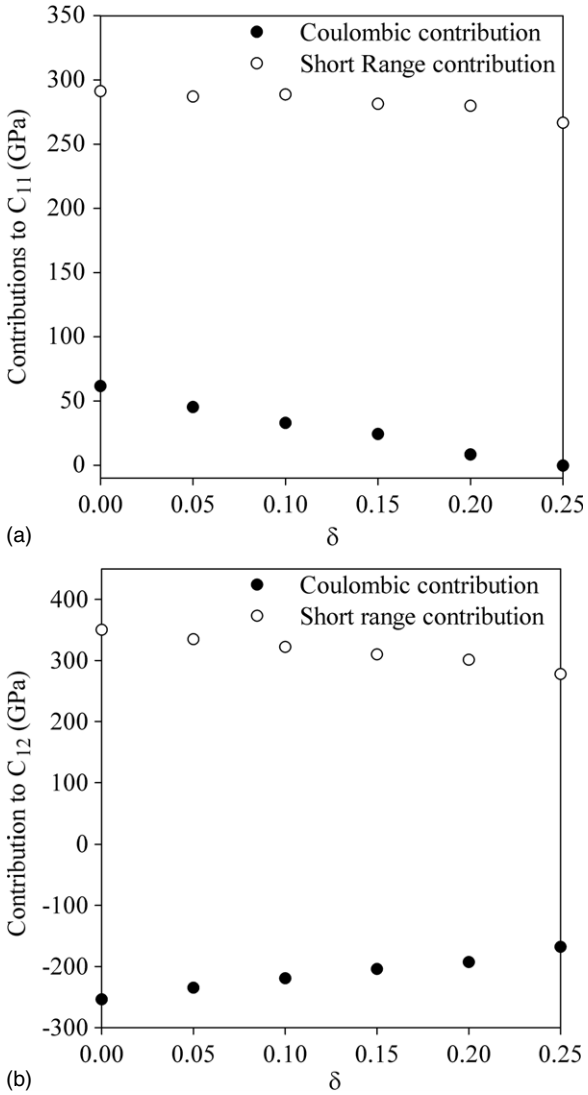

Figure 6. (*a*) Contribution from long-range and short-range parts of the interatomic potential towards C_{11}. (*b*) Contribution from long-range and short-range parts of the interatomic potential towards C_{12}.

analyses performed showed a similar trend for the entire range of non-stoichiometry and temperature. Hence, we report the behavior for 1273 K, 20GDC only. In figure 6(*a*) we show the relative contributions from the coulombic and the short-range forces to the elastic constant C_{11}. It can be seen that the contribution of the long-range coulombic sum to the elastic constants is relatively small when compared to the contributions from the short-range part. Moreover, both contributions decreased with non-stoichiometry.

The same type of data is shown in figure 6(*b*) for C_{12}. From the figure it is clear that the relative magnitudes of the contributions are comparable. Further, with increasing vacancy concentration, the short-range contribution decreases while the coulombic contribution

increases. From this we can infer that the variation of total C_{12} (coulombic + short-range contributions) with the vacancy concentration is small and this explains the results in figure 3. A similar trend was observed for C_{66} as well (not shown).

5. Summary and conclusions

By using a semi-analytical approach in conjunction with MD simulations, the CCE and elastic constants of reduced 10 and 20GDC were determined over a range of non-stoichiometry and temperatures. The MD simulations were conducted on periodic simulation cells of defective 10 and 20GDC that were constructed using a new approach to allow for the calculation of inner-elastic constants. It was shown that the relaxed structure obtained after the simulations was such that the atoms were on, or close to locations which were a center of inversion. Thus the contribution from the inner-elastic constants was negligible. This study seems to indicate that the internal relaxation in defective 10 and 20GDC significantly altered the structure to an extent that defective fluorite modules as in [38, 39] may not be used to construct reduced non-stoichiometric ceria.

Our numerical results show that the compositional strain can be approximated as a linear function of non-stoichiometry following Vegard's law, and the corresponding CCE was found to be in the range of 0.069–0.079.

Over the range of non-stoichiometry examined, the elastic constant C_{11} was found to decrease significantly while C_{12} and C_{66} did not vary as much. Reasons for this behavior were partially given by examining the contributions from the short range and the coulombic portions to the elastic constants. It was observed that the variations of the contributions to C_{12} and C_{66} occurred with opposite slopes of almost equal magnitudes and thus did not cause a significant variation in C_{12} or C_{66} with vacancy concentration. Thus for single crystalline defective GDCs it is sufficient to consider only the variation of C_{11} to study the elastic response at varying levels of non-stoichiometry.

The averaged polycrystalline elastic constants were determined by considering an assembly of single crystals with random orientations. The corresponding Young's modulus and Poisson's ratio were calculated. It was found that for defective GDC structures made of polycrystalline material it is sufficient to consider only the variation of Young's modulus while modeling the interactions between defect transport and mechanics in GDC as the variation in Poisson's ratio was negligibly small.

Finally, it is found that neither CCE nor elastic modulus is sensitive to temperature.

Acknowledgments

The research was partially supported by NSF (CMMI 0726286). JQ also acknowledges the support of a visiting professorship from Harbin Institute of Technology (HIT) and valuable discussions with Professor Yi Sun and Mr Zhiwei Cui of HIT.

References

[1] Atkinson A 1997 *Solid State Ion. Diffus. React.* **95** 249
[2] Atkinson A and Ramos T M G M 2000 *Solid State Ion. Diffus. React.* **129** 259
[3] Duncan K L, Yanli W, Bishop S R, Ebrahimi F and Wachsman E D 2006 *J. Am. Ceram. Soc.* **89** 3162
[4] Swaminathan N, Qu J and Sun Y 2007 *Phil. Mag.* **87** 1705
[5] Larche F and Cahn J W 1973 *Acta Metall.* **21** 1051
[6] Chen Z 2004 *J. Electrochem. Soc.* **151** A1576

[7] Liu M 1997 *J. Electrochem. Soc.* **144** 1813
[8] Sato K, Hashida T, Yashiro K, Yugami H, Kawada T and Mizusaki J 2005 *J. Ceram. Soc. Japan* **113** 562
[9] Larche F and Cahn J W 1978 *Acta Metall.* **26** 53
[10] Larche F C 1988 *Diffus. Defect Data, Solid State Data, Part B (Solid State Phenom.)* **B3–B4** 205
[11] Larche F C and Cahn J W 1978 *Acta Metall.* **26** 1579
[12] Larche F C and Cahn J W 1982 *Acta Metall.* **30** 1835
[13] Larche F C and Cahn J W 1985 *Acta Metall.* **33** 331
[14] Larche F C and Voorhees P W 1996 *Diffus. Defect Data Part A Defect Diffus. Forum* **129–130** 31
[15] Johnson W C 1993 *J. Am. Ceram. Soc.* **76** 1713
[16] Johnson W C 1994 *J. Am. Ceram. Soc.* **77** 1581
[17] Yasuda I and Hishinuma M 1998 Electrical conductivity, dimensional instability and internal stresses of CeO_2–Gd_2O_3 solid solutions *Electrochemical Society Proc.* vol 97 pp 178–87
[18] Montross C S, Yokokawa H and Dokiya M 2002 *Br. Ceram. Trans.* **101** 85
[19] Mogensen M, Lindegaard T and Hansen U R 1994 *J. Electrochem. Soc.* **141** 2122
[20] Chen X, Yu J and Adler S B 2005 *Chem. Mater.* **17** 4537
[21] Adler S B 2001 *J. Am. Ceram. Soc.* **84** 2117
[22] Ebrahimi F, Yanli W, Duncan K and Wachsman E D 2007 *Solid State Ion. Diffus. React.* **178** 53
[23] Duncan K L, Wang Y, Bishop S R, Ebrahimi F and Wachsman E D 2007 *J. Appl. Phys.* **101** 044906
[24] Hayashi H, Kanoh M, Quan C J, Inaba H, Wang S, Dokiya M and Tagawa H 2000 *Solid State Ion.* **132** 227
[25] Hayashi H, Sagawa R, Inaba H and Kawamura K 2000 *Solid State Ion.* **131** 281
[26] Smith W and Forester T R 1996 *J. Mol. Graphics* **14** 136
[27] Vyas S, Grimes R W, Gay D H and Rohl A L 1998 *J. Chem. Soc.—Faraday Trans.* **94** 427
[28] Gotte A, Spanberg D, Hermansson K and Baudin M 2007 *Solid State Ion.* **178** 1421
[29] Minervini L, Zacate M O and Grimes R W 1999 *Solid State Ion.* **116** 339
[30] Dingreville R and Qu J 2007 *Acta Mater.* **55** 141
[31] Wang Y L, Duncan K, Wachsman E D and Ebrahimi F 2007 *Solid State Ion.* **178** 53
[32] Wachsman E D 2004 *J. Eur. Ceram. Soc.* **24** 1281
[33] Guttman L 1956 *Solid State Phys.—Adv. Res. Appl.* **3** 145
[34] Born M and Huang K 1954 *Dynamical Theory of Crystal Lattices* (Oxford: Clarendon)
[35] Alber I, Bassani J L, Khantha M, Viter V and Wang G J 1992 *Phil. Trans. R. Soc.* A **339** 555
[36] Martin J W 1975 *J. Phys. C: Solid State Phys.* **8** 2858
[37] Jianmin Q and Cherkaoui M 2006 *Fundamentals of Micromechanics of Solids* (New York: Wiley)
[38] Krivovichev S V 1999 *Solid State Sci.* **1** 221
[39] Krivovichev S V 1999 *Solid State Sci.* **1** 211
[40] Kang Z C and Eyring L 1997 *J. Alloys Compounds* **249** 206